

BIO-FLEXCLC**Flexible chemical looping combustion for combined heat and power production from
biogenic residues with negative emission****HORIZON EUROPE GRANT AGREEMENT NUMBER: 101147904**

Start date of project: 01/06/2024

Duration: 4 years

WP2**Improving process performance of flexible Bio-CLC****D2.3****Optimization of the post-oxidation chamber design
by CFD modelling**

Topic: HORIZON-CL5-2023-D3-02-01
Funding scheme: HORIZON-RIA
Call identifier: HORIZON-CL5-2023-D3-02-01

Due date of deliverable: 31-05-2025	Actual submission date: 28-05-2025	Reference period: 01-06-2025 – 31-05-2025
Document classification code: Bio-FlexCLC-WP02-D2.3-DLR-CERTH-280525-V04		Prepared by: CERTH

Version	DATE	Changes	CHECKED	APPROVED
V01	2025-04-07	First Release	CERTH	Theodoros Lyras
V02	2025-05-10	Added final results	CERTH	Theodoros Lyras
V03	2025-05-25	Incorporated review comments from partners	CERTH	Theodoros Lyras
V04	2025-05-28	Final version	RISE	Amir Soleimani Salim

Funded by the European Union. Views and opinions expressed are however those of the author(s) only and do not necessarily reflect those of the European Union or the European Climate, Infrastructure and Environment Executive Agency (CINEA). Neither the European Union nor CINEA can be held responsible for them."

Dissemination Level		
PU	Public	X
SEN	Sensitive, limited under the conditions of the Grant Agreement	



D2.3 - Optimization of the post-oxidation chamber design by CFD modelling

Proj. Ref.: Bio-FlexCLC-101147904
Doc. Ref.: Bio-FlexCLC-WP02-D2.3-DLR-CERTH-280525-V04
Date: 28/05/2025
Page N°: 2 of 26

Content

1. EXECUTIVE SUMMARY (3 pages max. all points)	3
1.1. Description of the deliverable content and purpose	3
1.2. Brief description of the state of the art and the innovation brought	3
1.3. Deviation from objectives	3
2. METHODOLOGY	4
2.1. Models and Assumptions	4
2.2. Specifications and boundary conditions	5
2.2.1. Chalmers University of Technology (CTH).....	5
2.2.2. Spanish National Research Council (CSIC).....	7
2.2.3. Technical University of Darmstadt (TUDA)	9
3. CFD MODELLING RESULTS	11
3.1. CFD modelling of CTH post-oxidation chamber designs	11
3.1.1. Top-feed fuel injection	11
3.1.2. Bottom-feed fuel injection	12
3.1.3. Comparative results	15
3.2. CFD modelling of CSIC post-oxidation chamber designs	18
3.2.1. Low wall temperature (700 °C)	18
3.2.2. High wall temperature (1000 °C).....	19
3.2.3. Comparative results	20
3.3. CFD modelling of TUDA post-oxidation chamber designs	21
3.3.1. A – Installed Cooling System.....	21
3.3.2. B – Refractory (adiabatic) wall.....	22
3.3.3. Comparative results	24
4. CONCLUSIONS	25
5. ABBREVIATIONS	25
6. REFERENCES	26

1. EXECUTIVE SUMMARY

1.1. Description of the deliverable content and purpose

The present report describes the carried out work corresponding to Task 2.2, titled “*CFD modelling of various designs for post-oxidation chamber*”. The aim of said task was to provide design specifications for the post-oxidation chambers that will be utilized in Tasks 2.4 (10 kW_{th} and 20 kW_{th} pilot-plants) and 4.1 (1 MW_{th} Bio-CLC plant). The main work was carried out by the Centre for Research and Technology, Hellas (CERTH), while Chalmers University of Technology (CTH), the Spanish National Research Council (CSIC) and Technical University of Darmstadt (TUDA) provided necessary feedback regarding initial post-oxidation chamber (POC) specifications. Based on the input provided by CTH, CSIC and TUDA, CERTH performed computational fluid dynamics (CFD) simulations of various post-oxidation chamber designs. The main targets of the CFD campaign were to establish whether the oxidation process would be efficient and, to assess if high-temperature areas would be present in the chamber. Moreover, the concept of air staging was implemented and tested. For all examined POC designs, there is a large number of data produced that is available to all involved partners and stakeholders.

This report comprises four main paragraphs. The current paragraph states the main target of the performed work, presents a brief description regarding the state of the art in combustion modelling, comments briefly on the produced results and closes by reporting the deviations (if any) from the initial objectives. Paragraph “**2.METHODOLOGY**” describes the numerical models that have been employed for the POC simulation, along with any relevant settings, assumptions and justifications. A validation case of the finalised POC CFD model is also presented. The main results of the numerical campaign are presented in the paragraph “**3.CFD MODELLING RESULTS**”. Five different POC designs are evaluated, and the corresponding results are presented in terms of temperature distribution, heat flux and species concentration depending on the case. Finally, paragraph “**4.CONCLUSIONS**”, summarizes the main findings of the CFD campaign.

1.2. Brief description of the state of the art and the innovation brought

- Oxy-fuel oxidation CFD model for methane and ethylene containing gas mixture.
- A reaction mechanism comprising 8 species and 5 chemical reactions.
- Use of a methane oxidation mechanism modified for oxy-fuel combustion.
- Discrete Ordinates radiation heat transfer modelling and use of weighted-sum-of-gray-gases model (WSGGM).
- Adequately dense mesh in the near-wall region, with a dimensionless distance, y^+ , equal to 1.

1.3. Deviation from objectives

There has been no deviation from the initial objectives that needs to be reported.

2. METHODOLOGY

2.1. Models and Assumptions

The analysis and evaluation of the POC design have been conducted with the use of the commercial CFD software ANSYS Fluent. After the initial deliberation regarding the CFD modelling options, a two-dimensional, axisymmetric approach was chosen in order to allow for an agile and fast initial model testing, design evaluation and, eventually, the subsequent testing of different operating set-ups. The pressure-based solver was utilized, and a transient formulation was adopted, as the system's dynamic response can be of interest in terms of design. Gravitational acceleration effects were considered within the domain, and the field was set according to the orientation of the examined unit. Turbulent effects inside the POC domain were accounted for, using a Reynolds-averaged Navier-Stokes (RANS) framework with the utilisation of the k- ω , shear stress transport (SST) turbulence model. The choice of the specific model was made because of its ability to handle adverse pressure gradients, possible recirculation and flow detachment [1]. Moreover, the desired near-wall mesh resolution dictated that no wall-functions would be used for resolving the boundary layer region. Instead, an adequately dense mesh was used for the near-wall region, with a dimensionless distance, y^+ , equal to 1. This value ensures that the thermal and the velocity boundary layers are resolved. For example, for the range of operating conditions of the POC units examined in the TUDA campaign, the flow was fully turbulent as the Reynolds number, Re , was approximately 23000, as shown in **Equation 1**.

$$Re = \frac{\rho UD}{\mu} = 22\,812 \quad \text{Equation 1}$$

Where $\rho = 0.261 \text{ kg/m}^3$, $U = 15.11 \text{ m/s}$, $D = 0.25 \text{ m}$, and $\mu = 4.322 \times 10^{-5} \text{ Pa}\cdot\text{s}$, are the density, the average stream velocity, the domain diameter and the dynamic viscosity, respectively. The aforementioned Reynolds number yields a cell-to-wall distance for the first layer of cells of approximately **0.15 mm**, which was the cell size that was used in the numerical meshes of the specific campaign. The near-wall mesh size was calculated for all examined POC units accordingly.

An important aspect of the POC modelling is the representation of the chemical reactions of the oxidation process that takes place within the unit. In order to model such processes with high accuracy, extensive reaction mechanisms are needed. However, these types of detailed reaction mechanisms contain a large number of species and an even larger number of chemical reactions. Indicative examples of detailed chemical kinetic models (DCKM) are presented in **Table 1**.

Table 1. Detailed combustion mechanisms available in the literature.

Mechanism	Species	Reactions	Affiliation	Year	Comments
GRI-Mech 3.0	53	325	-	1999	H ₂ -CH ₄ combustion
San Diego	57	268	UC San Diego	2005	H ₂ -CH ₄ -C ₂ H ₄ -C ₃ H ₈ -C ₄ H ₁₀ combustion
USC II	111	784	University of Southern California	2007	H ₂ -CO-C ₁ to C ₄ combustion
Konnov (v0.6)	201	2300	-	2009	CH ₄ plasma combustion
POLIMI C₁-C₃ mechanism	159	268	Politecnico di Milano	2015	Hydrocarbons from C ₁ to C ₃ combustion
NUIGMech1.1	-	-	National University of Ireland Galway	2020	C ₁ to C ₅ combustion

Although accurate, the computational cost of the above-presented mechanisms, when used in a CFD framework, is unrealistic. For practical design CFD applications, the use of simpler (global) reaction mechanisms has been adopted. Widely used global mechanisms are those presented by Jones and Lindstedt [2], and Westbrook and Dryer [3]. Those mechanisms model the combustion mechanism of hydrocarbons with the use of fewer oxidation steps in comparison to their detailed counterparts. For modelling the methane oxidation process in this work, a modified version of the Jones and Lindstedt model was used. The model was modified for oxy-fuel combustion by Andersen et al. [4]. Moreover, in the cases where ethylene is expected to be present in the gas flow from the fuel reactor, an additional reaction was included based in the publication of Peters and Rogg [5]. The final unified mechanism that was used for modelling of oxidation of mixtures containing methane and ethylene, consists of 8 species, namely O_2 , H_2 , N_2 , H_2O , CO , CO_2 , CH_4 , and C_2H_4 , and 5 chemical reactions (R1 to R5), which are presented in **Table 2**.

Finally, to account for heat transfer through radiation, the discrete ordinates (DO) model has been used. In addition, since in combusting flows that include CO_2 and H_2O species in the mixture, the absorption of radiation by said species plays an important role in heat transfer, the weighted-sum-of-gray-gases model (WSGGM), offered by Fluent software has been utilized.

Table 2. Simplified methane, ethylene oxidation mechanism.

Reactions	$k_R = A T^n \exp(-E_a / RT)$			Reaction orders
	A	n	E_a	
R1 $CH_4 + 0.5 O_2 \rightarrow CO + 2 H_2$	7.82×10^7	0	1.26×10^8	$[CH_4]^{0.5}[O_2]^{1.25}$
R2 $CH_4 + H_2O \rightarrow CO + 3 H_2$	3.00×10^5	0	1.26×10^8	$[CH_4][H_2O]$
R3 $H_2 + 0.5 O_2 \rightarrow H_2O$	5.00×10^{14}	-1	1.26×10^8	$[H_2]^{0.25}[O_2]^{1.5}$
R3b $H_2O \rightarrow H_2 + 0.5 O_2$	2.93×10^{14}	-0.877	4.1×10^8	$[H_2]^{-0.75}[O_2][H_2O]$
R4 $CO + H_2O \rightleftharpoons CO_2 + H_2$	2.75×10^6	0	8.37×10^7	$[CO][H_2O]$
R5 $C_2H_4 + O_2 \rightleftharpoons 2 CO + 2 H_2$	1.20×10^{10}	0	1.46×10^8	$[C_2H_4][O_2]$

2.2. Specifications and boundary conditions

According to Task 2.2., CERTH will evaluate specific post-oxidation chamber (POC) designs based on communication with the operators of the CLC-units that will be tested within the project, namely the Chalmers University of Technology (CTH), the Spanish National Research Council (CSIC) and finally, the Technical University of Darmstadt (TUDA). The aforementioned partners have provided CERTH with all the required specifications regarding each POC unit, such as spatial and technical prerequisites and limitations, manufacturing and geometrical considerations, initial and boundary conditions, range of operating conditions and fuel composition. Based on the provided information, a number of designs were evaluated for each facility. The evaluated designs per CLC-unit-operator are presented in the following paragraphs.

2.2.1. Chalmers University of Technology (CTH)

Based on the spatial constraints of the existing facility, as well as the need to facilitate particle capture in the future, an initial POC design was proposed by CTH and modified for CFD by CERTH. The examined domain is presented below in terms of geometric dimensions in **Figure 1a** and numerical grid structure in **Figure 1b**. The chamber has a total volume of $0.0283 m^3$. It is positioned vertically, and the oxygen inlet is fixed at the bottom of the unit. With a fixed oxygen inlet, two operating modes were tested. During the first tested mode, **mode A**, the gas flow from the fuel reactor, henceforth referred to as "fuel", is entering the POC from the top of the unit, while during the second tested mode, **mode B**, the fuel is entering from the bottom of the unit.

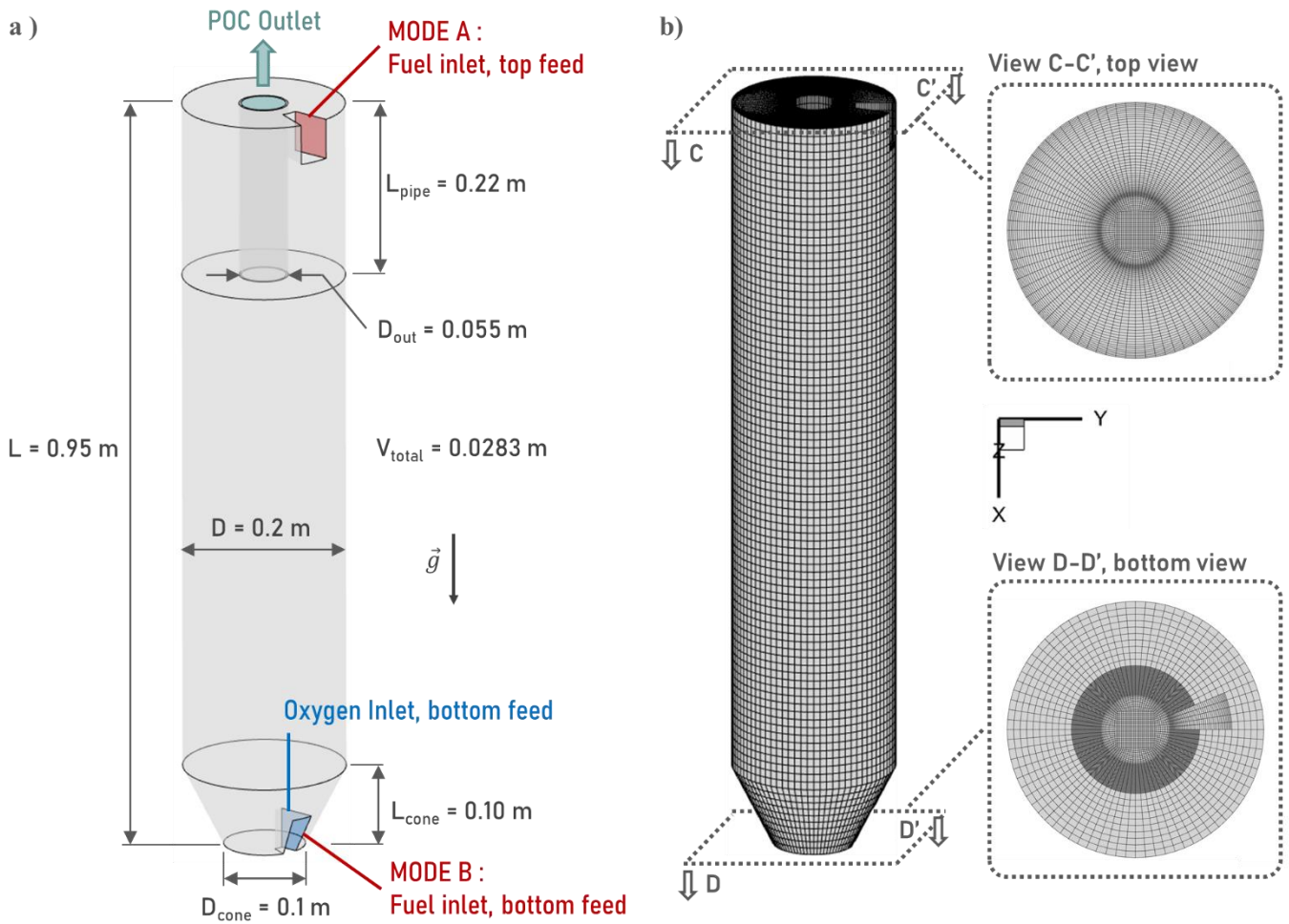


Figure 1. Post-oxidation chamber geometry for the CTH facility.

The 3D, numerical grid that was constructed, consists of structured topologies and comprises approximately 460000 hexahedral cells. For this 3D investigation, the near-wall resolution was calculated to be compatible with the use of wall functions. Thus, the Realizable $k - \varepsilon$ turbulence model was selected, along with standard wall functions.

The boundary conditions that were considered for both examined modes, A and B, are presented in **Table 3**. For each mode of operation, two flow rate scenarios are investigated, i.e., **scenario 1** where the volume flow rate of the incoming fuel is set to 255 Lmin^{-1} and, **scenario 2**, where the fuel volume flow rate is set to 401 Lmin^{-1} .

Table 3. Boundary conditions imposed for the POC evaluation of the CTH facility.

Boundary Conditions	Value
Inlet fuel (gas from Fuel Reactor) flow rate - Scenario 1 :	$255 [\text{L min}^{-1}]$
Inlet fuel flow rate - Scenario 2 :	$401 [\text{L min}^{-1}]$
Inlet fuel temperature	$950 [^{\circ}\text{C}]$
Inlet oxygen flow rate (Scenario 1 / 2)	$12 / 18 [\text{L min}^{-1}]$
Inlet oxygen temperature	$25 [^{\circ}\text{C}]$
Outlet pressure	$101325 [\text{Pa}]$

Finally, the composition of the fuel that is entering the POC is presented in **Table 4**.

Table 4. Fuel composition as expected to be received from the fuel reactor, expressed in molar fractions. Values provided by CTH.

Fuel species, i	Inlet molar fraction, X_i [-]
CH ₄	0.05
H ₂	0.02
CO	0.05
CO ₂	0.08
H ₂ O	0.60
N ₂	0.20

The data that resulted from the four simulations reported in this paragraph, namely of mode A, scenario-1 (A-1) and 2 (A-2) and of mode B, scenarios 1 (B-1) and 2 (B-2), are presented in **Paragraph 3.1**.

2.2.2. Spanish National Research Council (CSIC)

The 20 - 50 kW_{th} CLC unit that operates in the CSIC facility is depicted in **Figure 2**. The fuel reactor (FR) runs from the distributor plate to the cyclone, with a total length of 4 m. At a height of 1200 mm, there is a change in the dimensions, where the internal diameter of the reactor decreases from 102.3 mm to 80.9 mm. After the fuel reactor, the gas flow is entering the exit cyclone. The CSIC POC unit is planned to be fitted vertically, after the cyclone following the FR. Based on the experience and know-how of CSIC, to ensure the satisfactory oxidation of combustible species that will enter the POC, it is considered that additional heat should be provided to the walls of the chamber. Based on this scenario, it was agreed that the effect of the POC's wall temperature would be the subject of CERTH's numerical investigation.

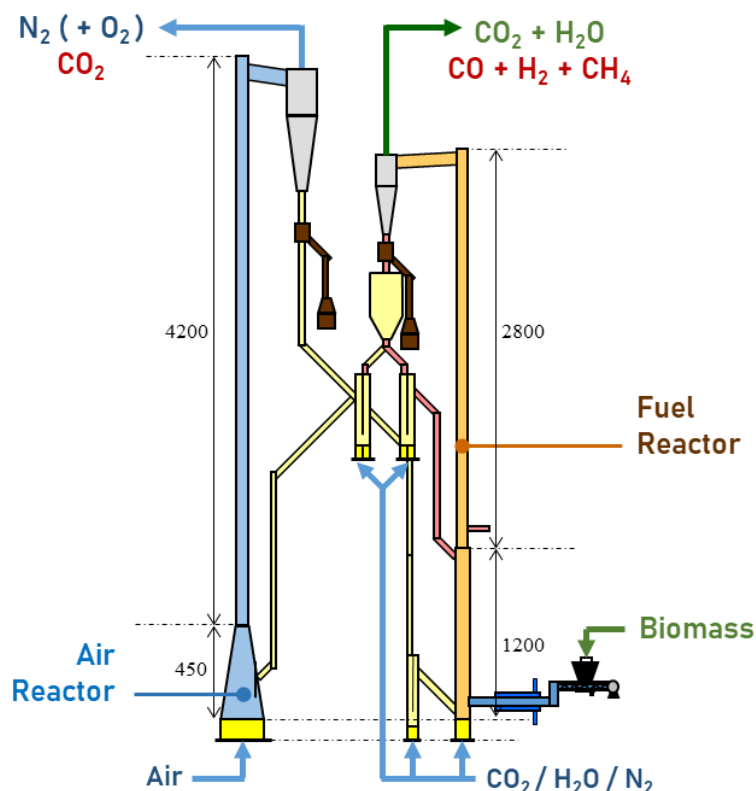


Figure 2. Schematic of the CSIC CLC unit. Measurements are reported in mm.

The examined domain is presented in **Figure 3** in terms of geometric dimensions and numerical grid structure. The chamber is positioned vertically, and the oxygen is entering the domain from the locations marked as “O₂ inlets” so as to also investigate the effect of injecting the oxygen in stages. The numbers over the inlets report the active inlets for each oxygen-staging configuration, e.g. for two oxygen injection points, the active inlets are the first and the third. The wall of the POC is considered to be heated to a constant temperature. In this numerical campaign, the examined temperatures were set to 700, 800, 900 and 1000 °C.

The 2D, numerical grid that was constructed, consists only of structured topologies and comprises approximately 60000 tetrahedral cells. For this investigation, the near-wall resolution was set to a cell size that would result to a dimensionless distance, y^+ , equal to 1, ensuring that the thermal and the velocity boundary layers are resolved. No wall functions were used, and turbulence was modelled with the use of the SST $k - \omega$ turbulence model. Heat transfer by radiation was modelled with the Discrete Ordinates (DO) model, and the radiation absorption by the gas phase was modelled using the weighted-sum-of-gray-gases model (WSGGM).

The boundary conditions that were considered for all examined cases are presented in **Table 5**. The fuel flow rate is approximately $267 L_n min^{-1}$ and the gas is entering the POC domain at a temperature of 900 °C. Regarding the oxygen inlets, it must be noted that no solid boundaries were introduced in the geometry, as this would cause unrealistic flow patterns within the chamber. Appropriate mass sources were introduced instead. The composition of the fuel entering the POC for all investigated cases is presented in **Table 6**. Finally, the simulation result from the heated-wall POC campaign, for different wall temperature values, i.e. 700, 800, 900, and 1000 °C are presented in **Paragraph 3.2**.

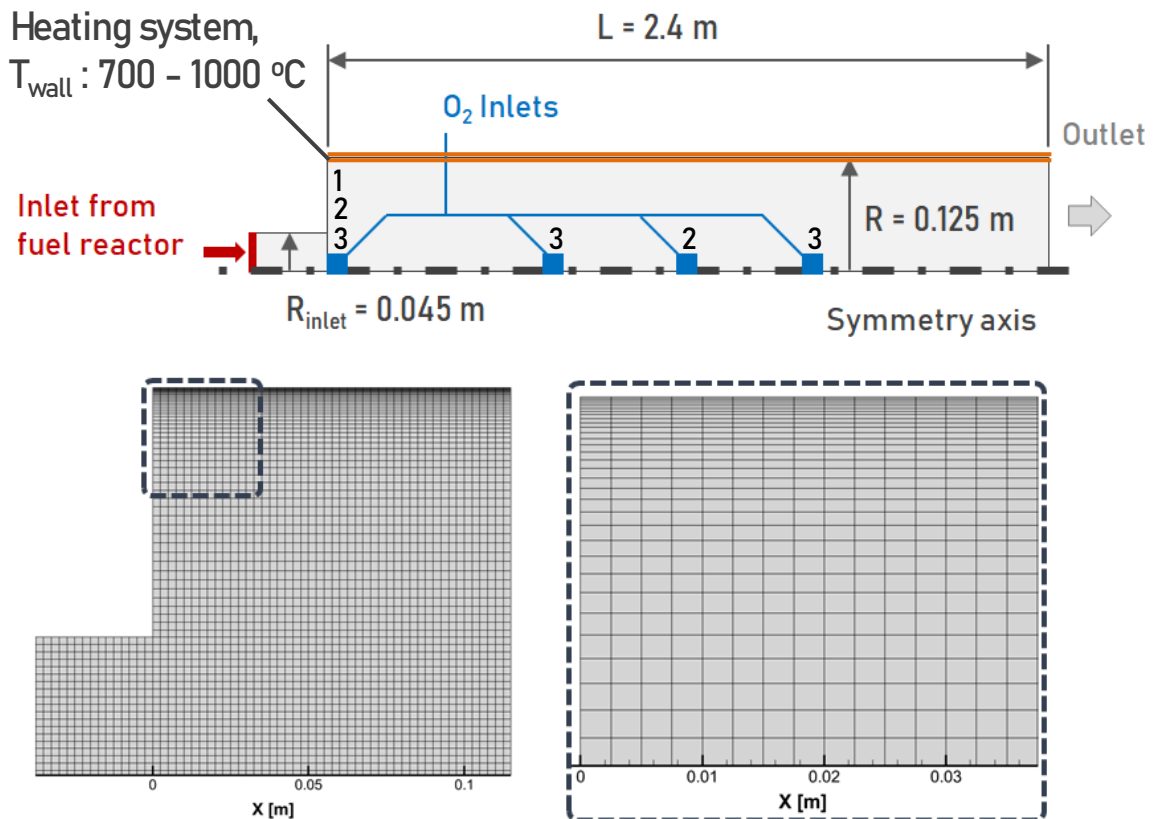


Figure 3. Post-oxidation chamber geometry for the CSIC facility.

Table 5. Boundary conditions imposed for the POC evaluation of the CSIC facility.

Boundary Conditions	Value
Inlet fuel (gas from Fuel Reactor) flow rate	267 [$L_n \text{ min}^{-1}$]
Inlet fuel temperature	900 [$^{\circ}\text{C}$]
Inlet oxygen flow rate	25 [$L_n \text{ min}^{-1}$]
Inlet oxygen temperature	25 [$^{\circ}\text{C}$]
Outlet pressure	101325 [Pa]

Table 6. Fuel composition as expected to be received from the fuel reactor, expressed in molar fractions. Values provided by CSIC.

Fuel species, i	Inlet molar fraction, $X_i [-]$
CH ₄	0.01
H ₂	0.01
CO	0.03
CO ₂	0.78
H ₂ O	0.14
N ₂	0.03

2.2.3. Technical University of Darmstadt (TUDA)

Based on know-how from relevant projects, and an operational CLC unit, two initial POC designs were proposed by TUDA and adjusted for CFD usage by CERTH. The two designs are presented in **Figure 4**.

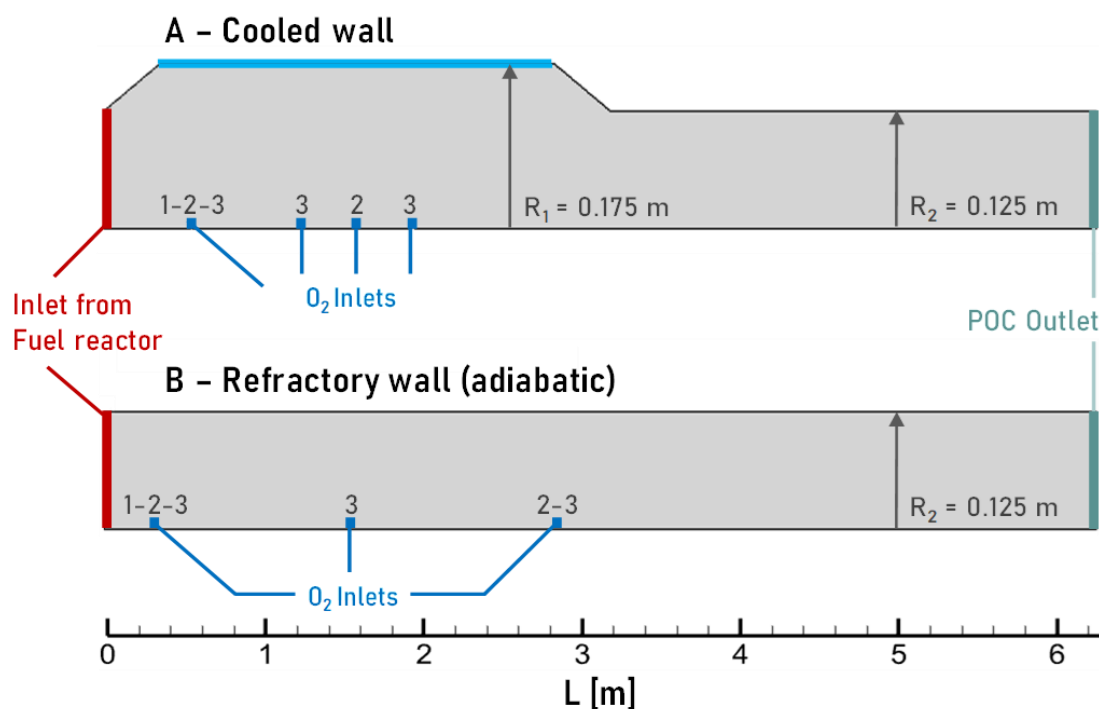


Figure 4. Post-oxidation chamber geometry for the TUDA facility.

The total length of the chamber for both designs is 6.25 m due to spatial restrictions. **Design A**, consists of a cooled part of 2.5 m and a radius of 0.175 m marked with light blue, followed by the non-isolated part without heat removal. The total volume of the POC is 0.441 m³ and is positioned vertically. Oxygen staging was investigated for this design by simulating one, two of three oxygen injection points as illustrated in the upper section of **Figure 4**. **Design B**, assumes an adiabatic wall condition throughout its length that will be achieved with the application of refractory wall material. The total volume of the POC is 0.308 m³ also positioned vertically. Oxygen staging was investigated for this design by simulating one, two, or three oxygen injection positions as illustrated in the lower section of **Figure 4**. The numerical grid that was constructed, is a 2D axisymmetric, structured mesh comprising approximately 62000 tetrahedral cells. As mentioned in **Paragraph 2.1**, an adequately dense mesh was used for the near-wall region, with a dimensionless distance, y^+ , equal to 1, ensuring that the thermal and the velocity boundary layers are resolved. No wall functions were used, and turbulence was modelled with the use of the SST $k - \omega$ turbulence model. Heat transfer by radiation was modelled with the Discrete Ordinates (DO) model. The boundary conditions that were considered for both examined designs, A and B, are presented in **Table 7**, while the composition of the fuel that is entering both POC designs is presented in **Table 8**.

Table 7. Boundary conditions imposed for the POC evaluation of the TUDA facility.

Boundary Conditions	Value
Inlet fuel (gas from Fuel Reactor) flow rate	650 [$L_n \text{ min}^{-1}$]
Inlet fuel temperature	850 [$^{\circ}C$]
Inlet oxygen flow rate (total)	155 [$L_n \text{ min}^{-1}$]
Inlet oxygen temperature	25 [$^{\circ}C$]
Outlet pressure	101325 [Pa]

Table 8. Fuel composition as expected to be received from the fuel reactor, expressed in molar fractions. Values provided by TUDA.

Fuel species, i	Inlet molar fraction, $X_i [-]$
C ₂ H ₄	0.0245
CH ₄	0.0315
H ₂	0.0315
CO	0.0280
CO ₂	0.2345
H ₂ O	0.6500
N ₂	-

The data that resulted from the simulations reported in this paragraph, namely of design A, and design B, are presented in **Paragraph 3.3**.

3. CFD MODELLING RESULTS

The final numerical campaign includes the evaluation of 5 different post-oxidation chamber (POC) configurations for 3 different CLC facilities and 24 sets of operating conditions. The results that are presented in this report are indicative and are selected with the purpose of highlighting the main findings of the campaign. The complete set of numerical data is available to Bio-FlexCLC partners.

3.1. CFD modelling of CTH post-oxidation chamber designs

In this paragraph, the results from the simulation of the proposed POC configuration corresponding to the CTH facility are presented.

3.1.1. Top-feed fuel injection

The figures included in this paragraph correspond to a top-fed POC unit, i.e., the gas from the fuel reactor is entering the chamber from the opening at the top. The oxygen is entering the chamber from the bottom. The results are presented in the form of contour plots over the plane of symmetry of the chamber ($Z = 0$ m). Based on the calculations and operational assumptions made by CTH, two volume flow rates were examined, a low volume flow rate of 225 Lmin^{-1} presented in **Figure 5**, and a high volume flow rate of 401 Lmin^{-1} presented in **Figure 6**. In both cases the calculated pressure drop is around 10 Pa . The velocity and density contours reveal for both cases that the fuel and oxygen mixing mostly takes place on the upper part of the chamber. Finally, the temperature within the domain is, for both cases, lower than the fuel injection temperature.

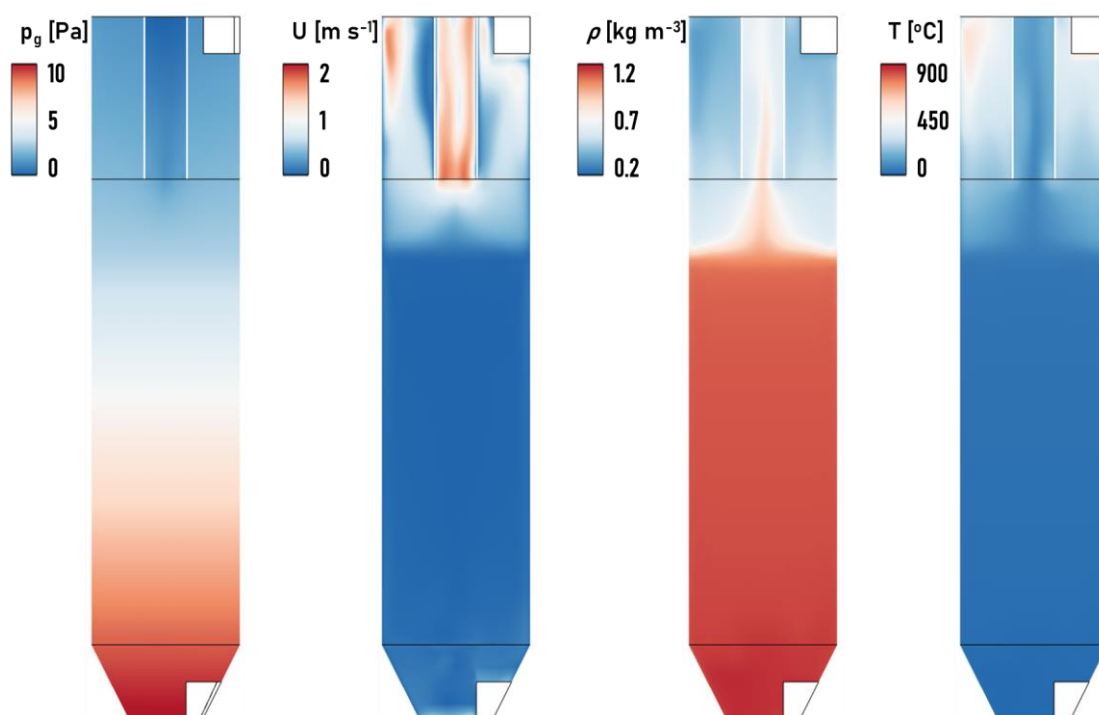


Figure 5. Contour plots of gauge pressure, p_g [Pa], velocity magnitude, U [ms^{-1}], gas phase density, ρ [kgm^{-3}], and temperature, T [$^{\circ}\text{C}$], on the plane of symmetry of the examined post oxidation chamber. Fuel inlet from the top right duct opening. Fuel volume flow rate from the fuel reactor: 255 Lmin^{-1} .

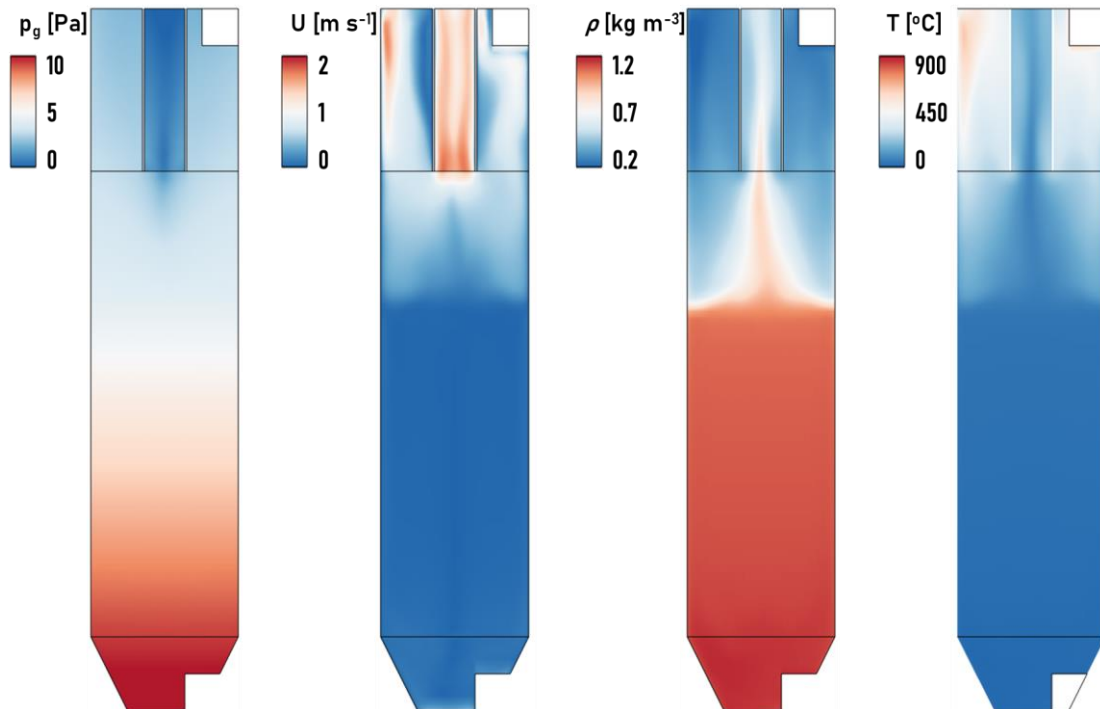


Figure 6. Contour plots of gauge pressure, p_g [Pa], velocity magnitude, U [$m s^{-1}$], gas phase density, ρ [$kg m^{-3}$], and temperature, T [$^{\circ}C$], on the plane of symmetry of the examined post oxidation chamber. Fuel inlet from the top right duct opening. Fuel volume flow rate from the fuel reactor: $401 Lmin^{-1}$.

3.1.2. Bottom-fed fuel injection

The figures included in this paragraph correspond to a bottom-fed POC unit, i.e. the gas from the fuel reactor is entering the chamber from a feeding duct at the bottom. The oxygen is entering the chamber from the bottom as well. The results are presented in the form of contour plots over the plane of symmetry of the chamber ($Z = 0 m$) Two volume flow rates were examined, a low volume flow rate of $225 Lmin^{-1}$, presented in **Figure 7**, and a high volume flow rate of $401 Lmin^{-1}$ presented in **Figure 9**. The main findings were that the bottom-fed chamber exhibits better mixing of fuel and oxygen, and more homogeneous temperature and density fields in comparison to its top-fed counterpart. However, the heat losses through the POC walls, play an important role in the chamber efficiency regardless the feeding topology. As was made clear by the numerical results, the temperature in the POC, both in top- and bottom-fed cases, does not exceed the fuel inlet temperature. This result indicates that the oxidation is not self-sustained and therefore, the options of wall insulation or the installation of a heat providing system may need to be explored. For this reason, two more simulations were set-up and executed. In those additional cases, the walls of the bottom-fed chamber were considered to be adiabatic, i.e. no heat flux is allowed through the POC walls, representing a theoretical chamber with perfect insulation and no heat losses. The corresponding results are presented in **Figure 8** for low flow rate and **Figure 10** for high flow rate. The insulated chamber results, especially the temperature contours, illustrate that chamber insulation is crucial for the oxidation reactions to advance. Due to the insulated walls, the gas temperature is not decreasing and upon contact with oxygen reacts faster, and leads to higher domain temperatures and a sustained oxidation process. The adiabatic case is a theoretic one, however, it highlights the need for insulation or equivalent wall heat source options to be considered.

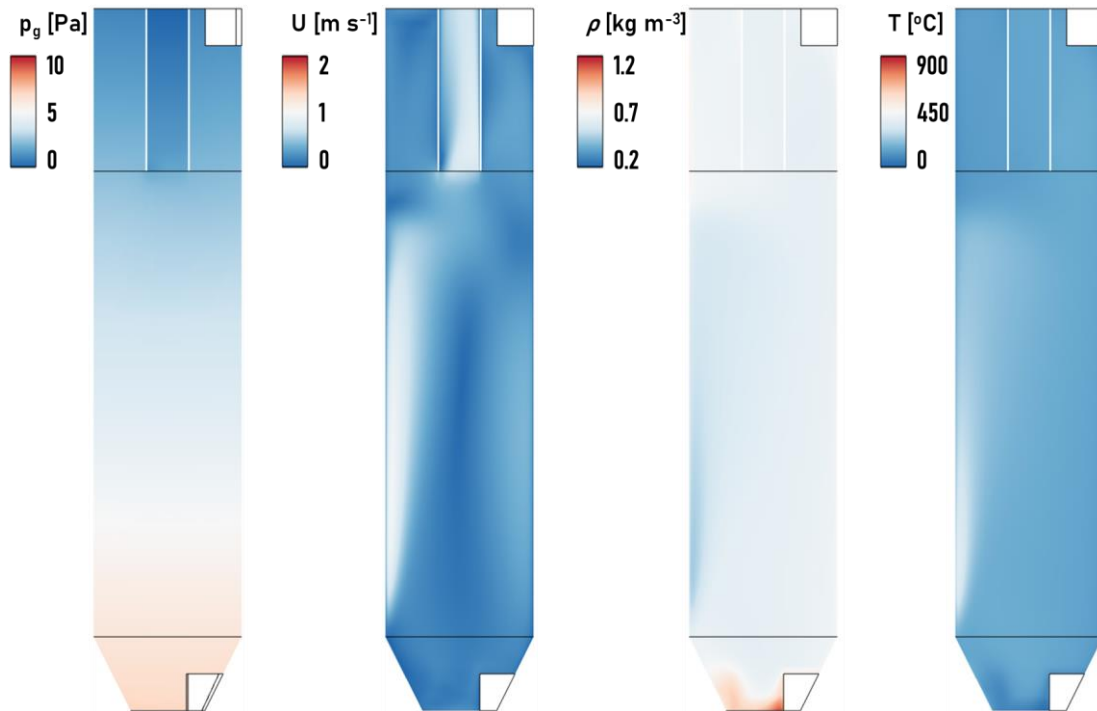


Figure 7. Contour plots of gauge pressure, p_g [Pa], velocity magnitude, U [ms^{-1}], gas phase density, ρ [kgm^{-3}], and temperature, T [$^{\circ}C$], on the plane of symmetry of the examined post oxidation chamber. Fuel inlet from the bottom right opening. Fuel volume flow rate from the fuel reactor: $255 Lmin^{-1}$.

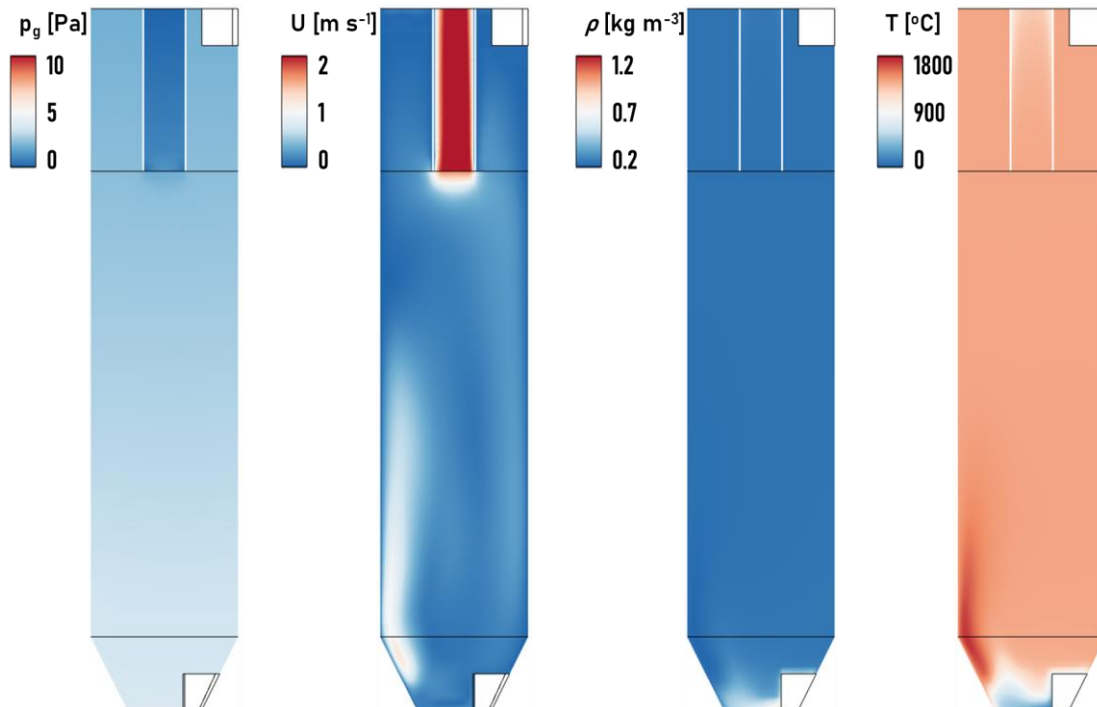


Figure 8. Contour plots of gauge pressure, p_g [Pa], velocity magnitude, U [ms^{-1}], gas phase density, ρ [kgm^{-3}], and temperature, T [$^{\circ}C$], on the plane of symmetry of the examined post oxidation chamber. Adiabatic walls. Bottom-fed chamber. Fuel volume flow rate from the fuel reactor: $255 Lmin^{-1}$.

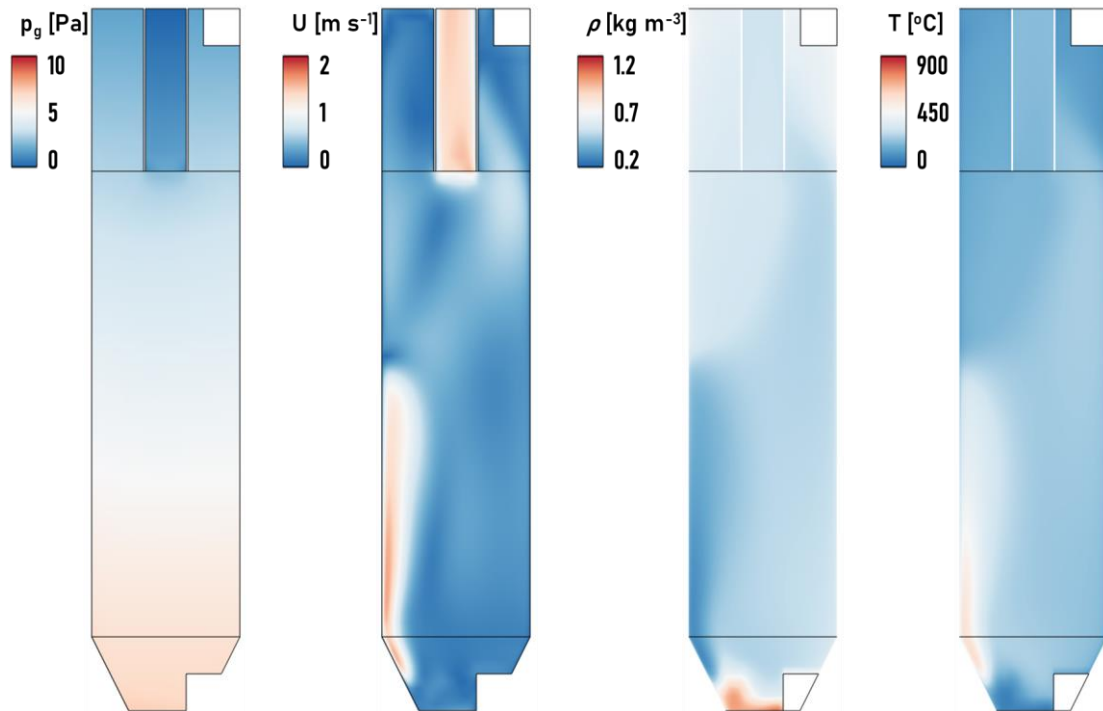


Figure 9. Contour plots of gauge pressure, p_g [Pa], velocity magnitude, U [ms^{-1}], gas phase density, ρ [kgm^{-3}], and temperature, T [$^{\circ}C$], on the plane of symmetry of the examined post oxidation chamber. Fuel inlet from the bottom right opening. Fuel volume flow rate from the fuel reactor: $401 Lmin^{-1}$.

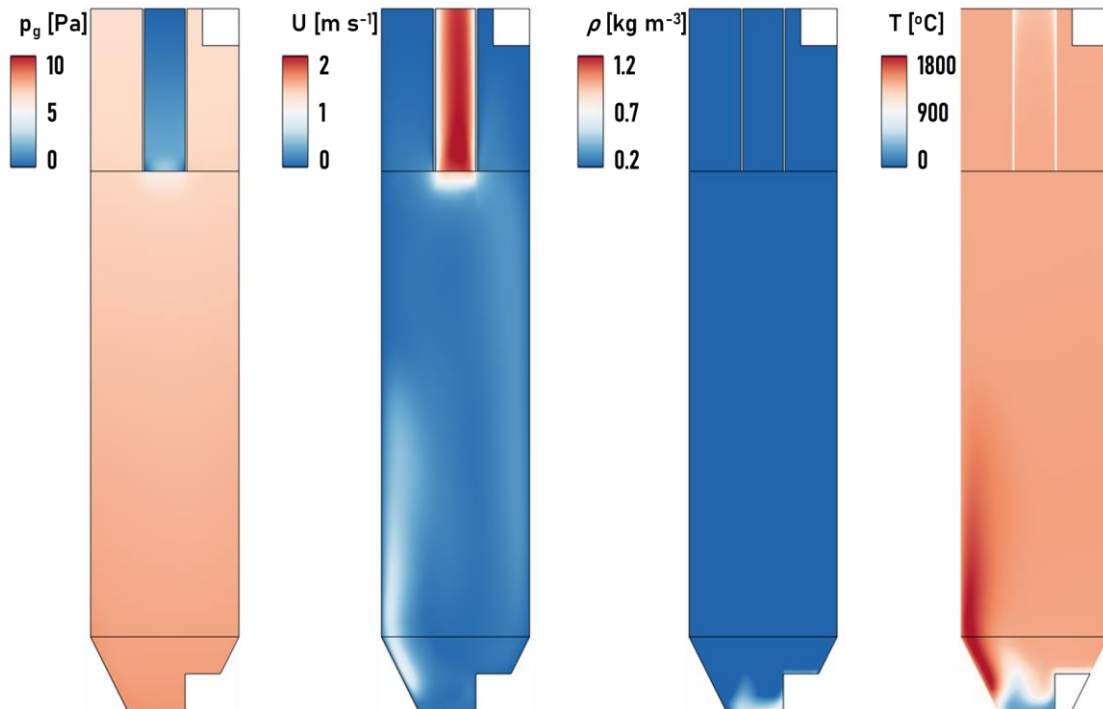


Figure 10. Contour plots of gauge pressure, p_g [Pa], velocity magnitude, U [ms^{-1}], gas phase density, ρ [kgm^{-3}], and temperature, T [$^{\circ}C$], on the plane of symmetry of the examined post oxidation chamber. Adiabatic walls. Bottom-fed chamber. Fuel volume flow rate from the fuel reactor: $401 Lmin^{-1}$.

3.1.3. Comparative results

To evaluate the simulated cases and draw conclusions regarding the examined POC designs, the produced numerical results are presented in this section comparatively. More specifically, **Figure 11** includes a comparison of the temperature fields for three POC configurations and for low and high volume flow rates. For each level of flow rate, the field corresponding to the top-fed chamber is placed on the left, the field corresponding to the bottom-fed chamber is placed in the middle, and the field corresponding to a bottom-fed chamber with adiabatic walls is placed to the right. In the case of the top-fed chamber, thermal stratification is observed due to pure mixing and the temperature difference of the injected fuel and oxygen. In the case of the bottom-fed chamber, the temperature field is more homogeneous, however, the fuel content is not enough to initiate a self-sustained oxidation reaction, as opposed to its adiabatic counterpart, where the theoretically insulated walls contribute to the temperature increase. The stratification in the case of the top-fed chamber is more evident in **Figure 12**, where the density contour reveals clearly the pure mixing of oxygen and fuel. **Figure 13** depicts velocity iso-surfaces with a value of 0.7 m/s. The mixing and any turbulent effects only take place at the upper part in the case of the top-fed chamber, as opposed to the elongated flow path in the case of the bottom-fed chambers, where a higher volume flow rate leads to higher flow swirl. Finally, **Figure 14** presents iso-surfaces of constant value of heat, Q_R [W], produced by the modelled chemical reactions in the areas where fuel and oxygen react. The plotted iso-surfaces are coloured by temperature level. In the case of the bottom-fed chamber, the iso-surfaces reveal a larger reaction surface that increases even more with the increase of the flow rate and the temperature.

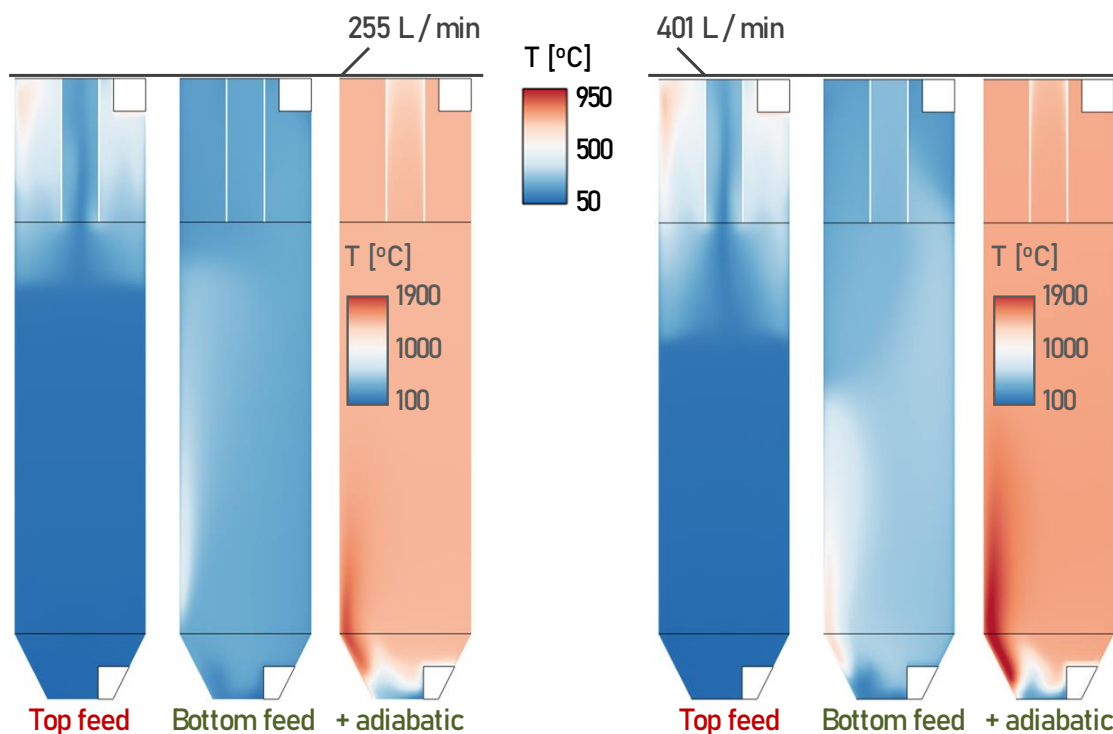


Figure 11. Contour plots of temperature, T [°C], for cases of low (left) and high (right) volume flow rate. Comparative view of a top-fed chamber, a bottom-fed chamber, and a bottom-fed chamber with adiabatic walls.

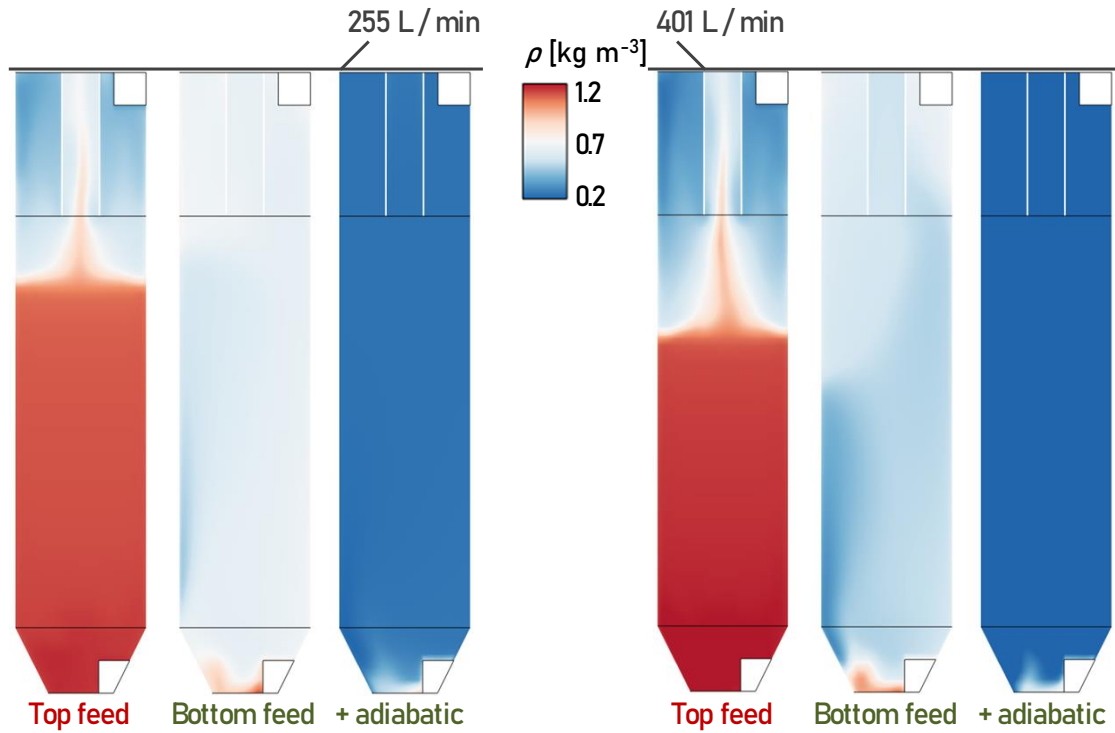


Figure 12. Contour plots of density, ρ [kg m^{-3}], for cases of low (left) and high (right) volume flow rate. Comparative view of a top-fed chamber, a bottom-fed chamber, and a bottom-fed chamber with adiabatic walls.

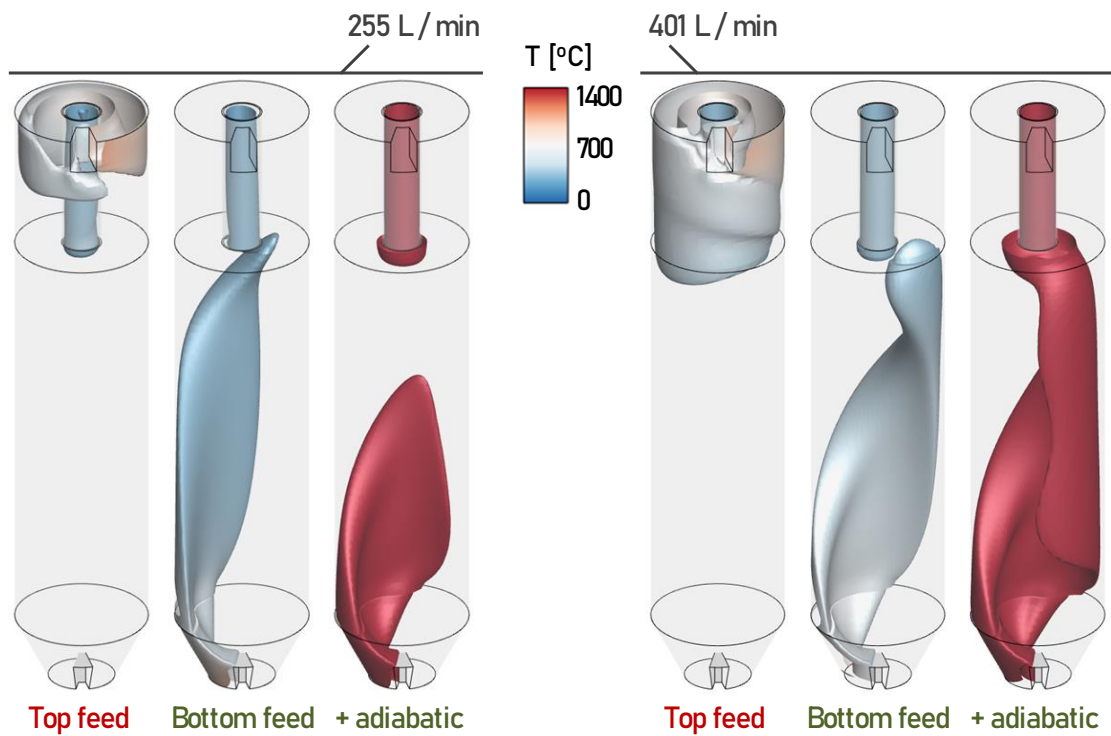


Figure 13. Iso-surface plots of velocity, coloured by temperature, T [$^{\circ}\text{C}$], for cases of low (left) and high (right) volume flow rate. Comparative view of a top-fed chamber, a bottom-fed chamber, and a bottom-fed chamber with adiabatic walls.

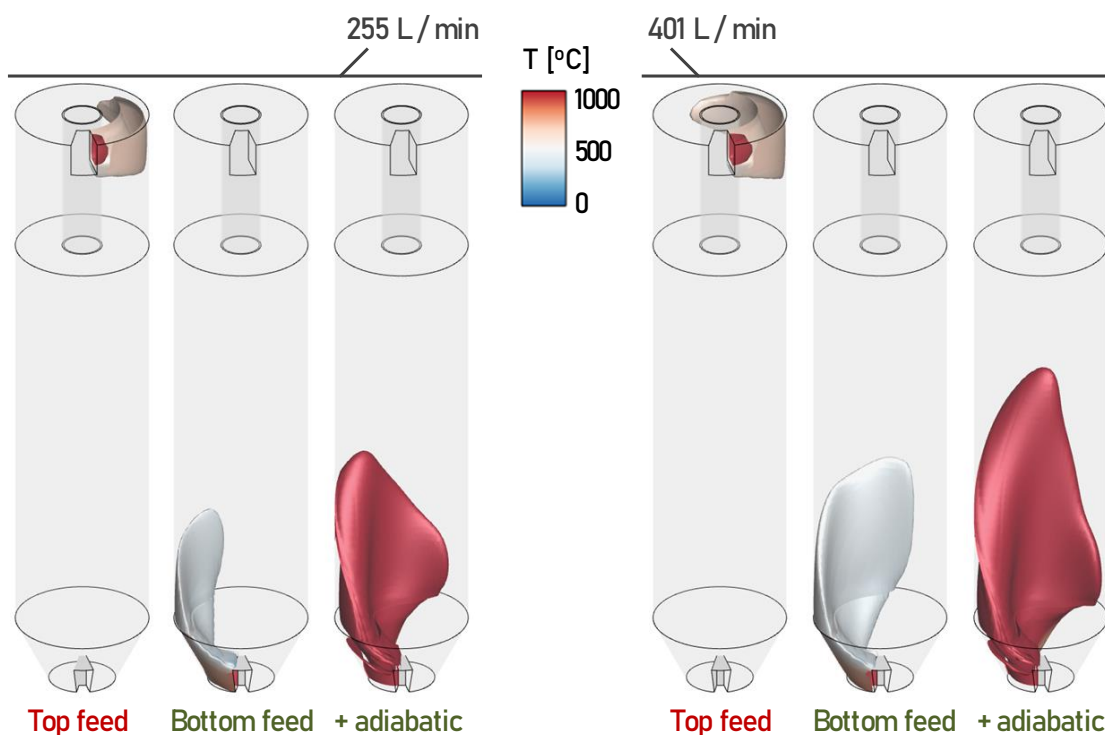


Figure 14. Iso-surface plots of heat of reaction, coloured by temperature, T [°C], for cases of low (left) and high (right) volume flow rate. Comparative view of a top-fed chamber, a bottom-fed chamber, and a bottom-fed chamber with adiabatic walls.

3.2. CFD modelling of CSIC post-oxidation chamber designs

The results from the simulation of the proposed POC configuration corresponding to the CSIC facility are presented in this paragraph. The numerical campaign based on the CSIC design examined cases of four different values of POC-wall temperature. The following paragraphs present simulation results from the lower, i.e. 700 °C, and higher, i.e. 1000 °C, wall temperature case, as well as a comparative evaluation of exported data.

3.2.1. Low wall temperature (700 °C)

The main purpose of the POC is to facilitate the oxidation of combustible species that may exit the fuel reactor, namely methane, hydrogen, and carbon monoxide. **Figure 15** and **Figure 16** present contour plots of CH_4 and CO_2 mole fraction in the POC for a wall temperature set to 700 °C and for 1, 2, or 3 oxygen injection points. Regardless of the oxygen injection stages, the total amount of oxygen injected is constant.

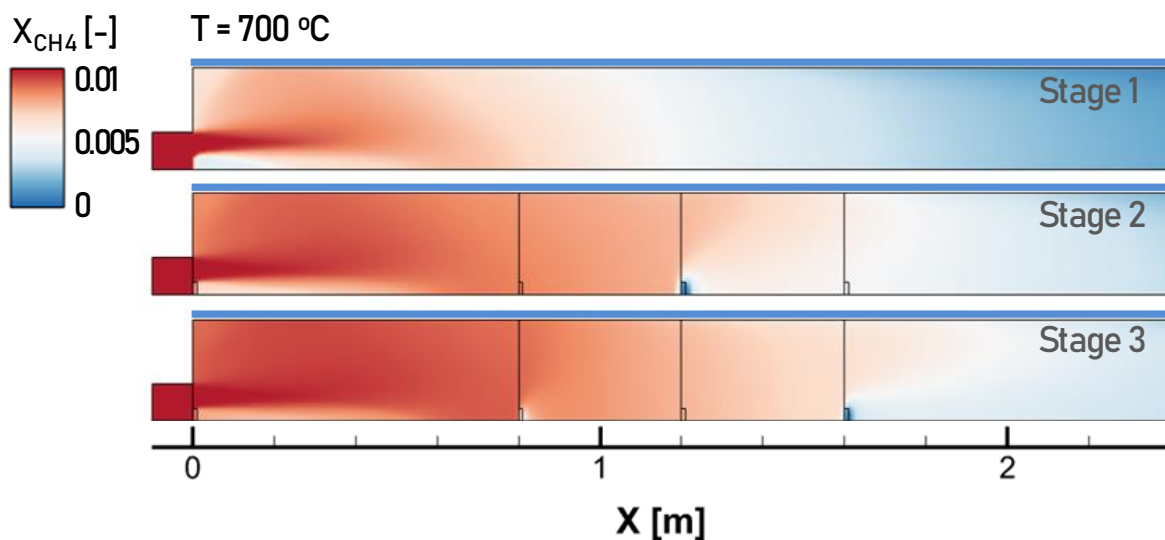


Figure 15. Methane mole fraction contours, X_{CH_4} [-], in the POC domain, at a wall temperature of 700 °C, for 1, 2, or 3 oxygen injection stages.

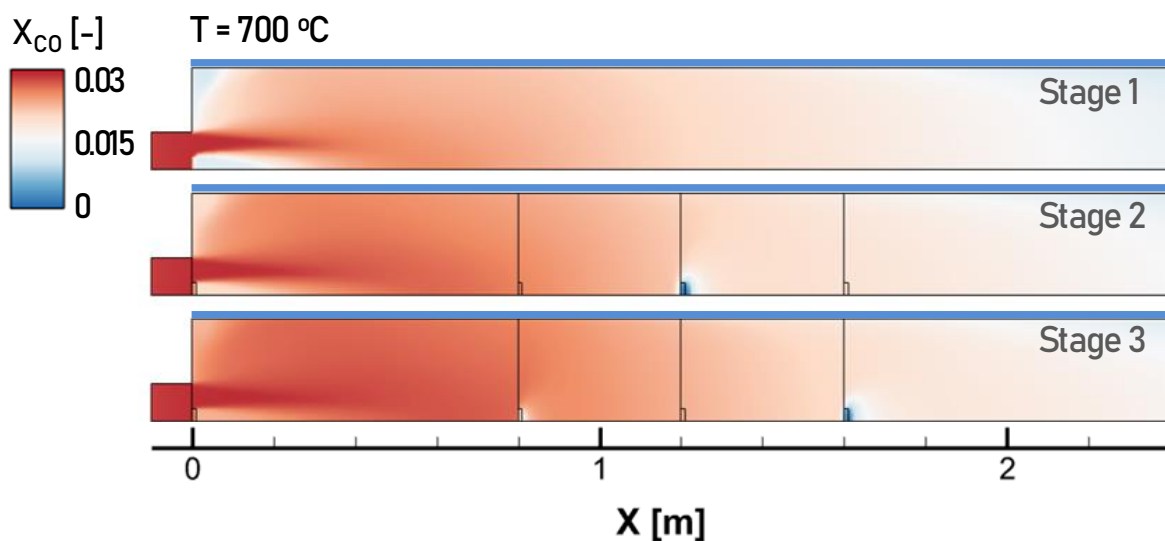


Figure 16. Carbon monoxide mole fraction, X_{CO} [-], in the POC domain, at a wall temperature of 700 °C, for 1, 2, or 3 oxygen injection stages.

The numerical simulations indicate that hydrogen oxidises fully into water vapour for all examined wall temperatures, while methane and carbon monoxide react more slowly, depending also on the additional heat provided to the system. **Figure 15** reveals that methane is present at the outlet of the POC for all three staging variations. The same applies to the presence of carbon monoxide, as depicted in **Figure 16**. Based on the results, it is safe to conclude that the oxidation process will not be complete without the addition of external heat in the system.

3.2.2. High wall temperature (1000 °C)

The high temperature wall boundary condition leads to heat being added to the system, raising the domain temperature and accelerating the modelled oxidation reactions. **Figure 17** and **Figure 18** present contour plots of CH₄ and CO₂ mole fraction in the POC for a wall temperature set to 1000 °C and for 1, 2, or 3 oxygen injection points. In the examined case, the mole fraction of both methane and carbon monoxide is zero, and the oxidation is complete.

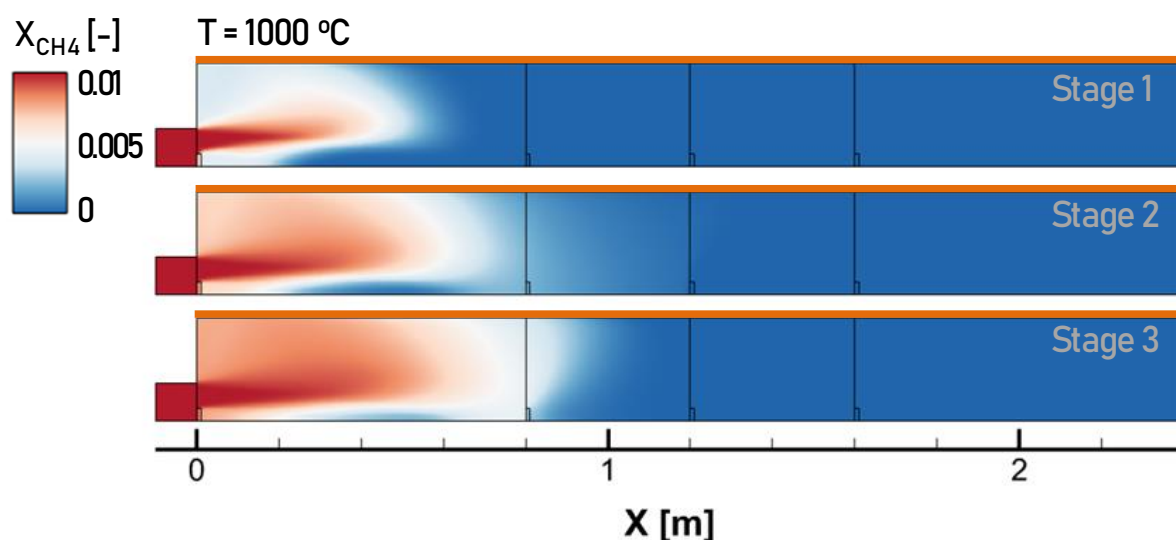


Figure 17. Methane mole fraction contours, X_{CH_4} [-], in the POC domain, at a wall temperature of 1000 °C, for 1, 2, or 3 oxygen injection stages.

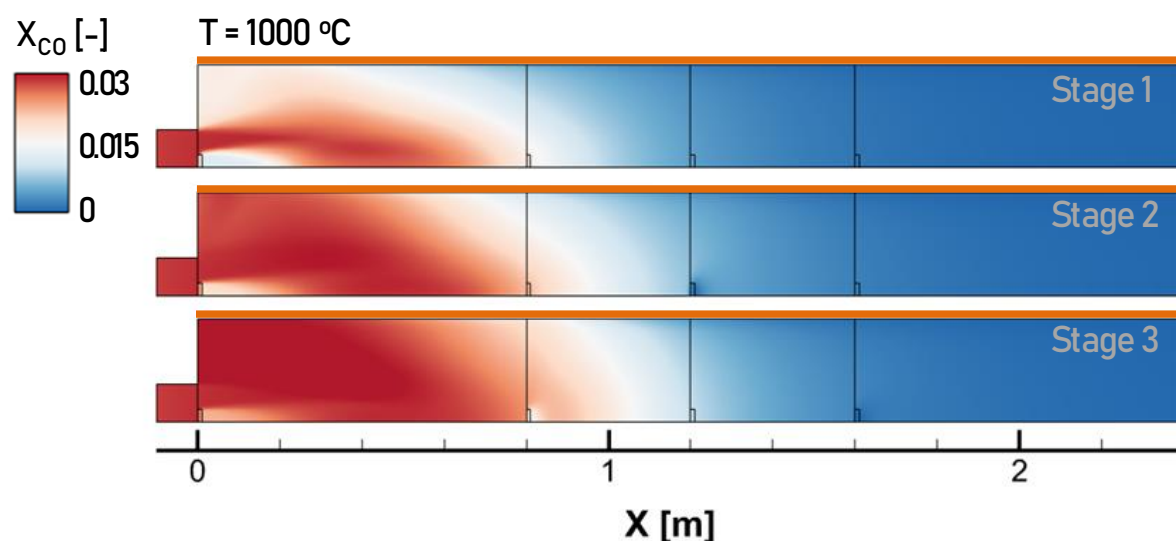


Figure 18. Carbon monoxide mole fraction, X_{CO} [-], in the POC domain, at a wall temperature of 1000 °C, for 1, 2, or 3 oxygen injection stages.

3.2.3. Comparative results

To evaluate the simulated cases and draw conclusions regarding the examined POC operating conditions, the produced numerical results are presented in this section comparatively. More specifically, **Figure 19** presents line plots of the value of CO_2 and H_2O mole fraction calculated at the outlet of the POC, for all examined wall temperatures and for 1, 2, and 3 stages of oxygen injection. It can be observed in said figure that the higher the wall temperature, the higher the content of the products of the oxidation process at the outlet of the chamber. As the wall temperature increases, more heat is entering the chamber and accelerates the oxidation reactions, increasing the fraction of CO_2 and H_2O in the gas flow. Further increase in wall temperature will not increase the CO_2 and H_2O content since there are no remaining combustible species. The impact of the wall temperature to the oxidation reaction intensity can be made clear in **Figure 20**, which presents line plots of the value of total heat produced by oxidation reactions as well as local cell value contours. As the wall temperature is set to a higher value, the heat produced by oxidation is increased, confirming that a higher wall temperature enhances the oxidation process.

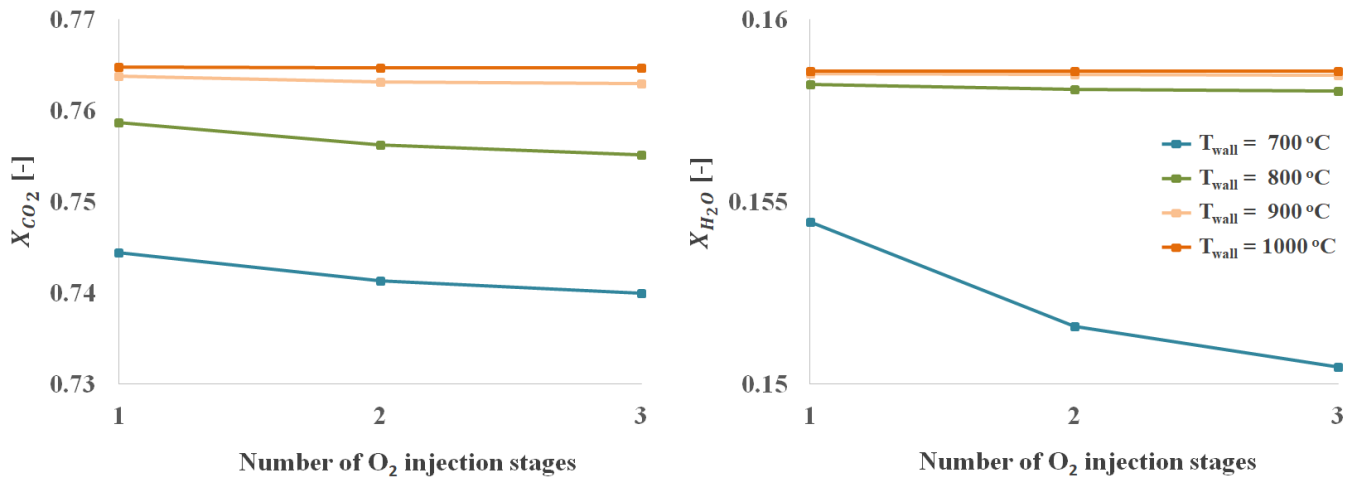


Figure 19. Line plots of CO_2 (left) and H_2O (right) mole fraction values at the outlet of the POC, for wall temperatures of 700, 800, 900, and 1000 °C, for 1, 2, and 3 stages of oxygen injection.

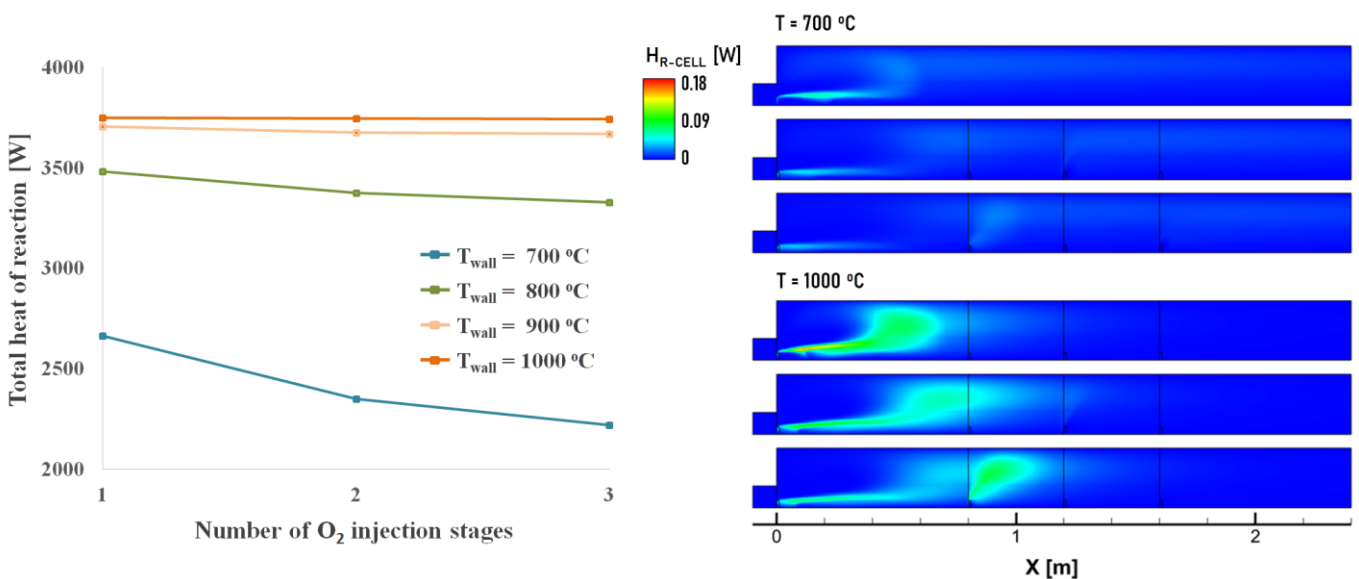


Figure 20. Line plots of the value of total heat produced by the modelled oxidation reactions within the POC domain, for wall temperatures of 700 and 1000 °C, for 1, 2, and 3 stages of oxygen injection.

3.3. CFD modelling of TUDA post-oxidation chamber designs

The results from the simulation of the proposed POC designs corresponding to the TUDA facility are presented in this paragraph. The operation conditions of the TUDA POC differ from the previous examined cases, in the sense that the content of the inlet flow in combustible material is higher and thus, the oxidation reactions are expected to release enough heat that would result in a self-sustained process that will increase the temperature of the chamber above the structure limits. Two possible approaches have been proposed by TUDA in order to avoid structural issues due to high wall temperatures. The first is the introduction of a cooling system on the first part of the chamber, and the second is the use of heat-resistant refractory material that will insulate the chamber, resulting, in terms of simulation, to an adiabatic wall treatment. The following paragraphs present simulation results from a POC design, including a cooling system and a POC design that features adiabatic walls as a result of the application of refractory material in the inner wall of the chamber. Finally, a comparative evaluation of selected simulation data is included.

3.3.1. A – Installed Cooling System

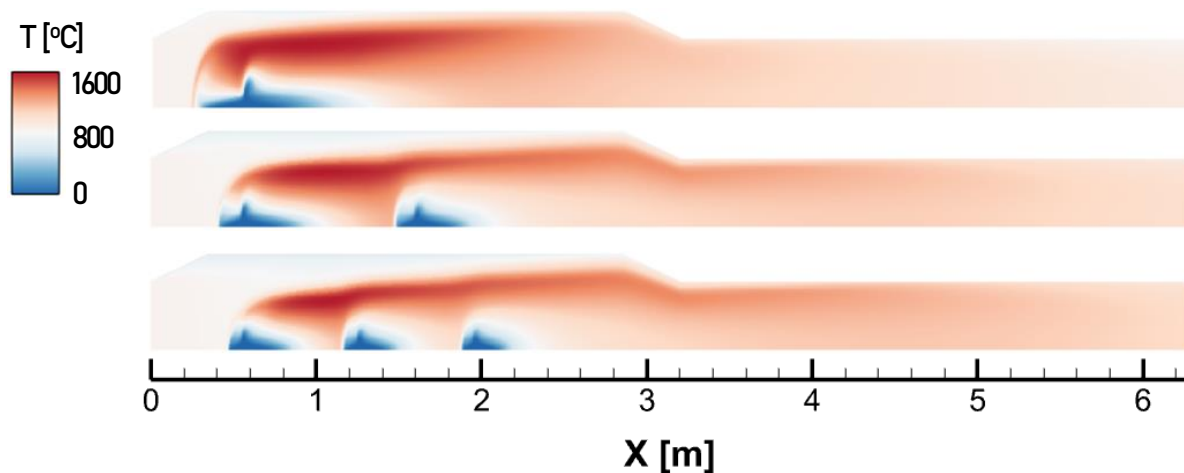


Figure 21. Contour plots of temperature in the cooled POC domain for 1, 2, or 3 oxygen injection stages.

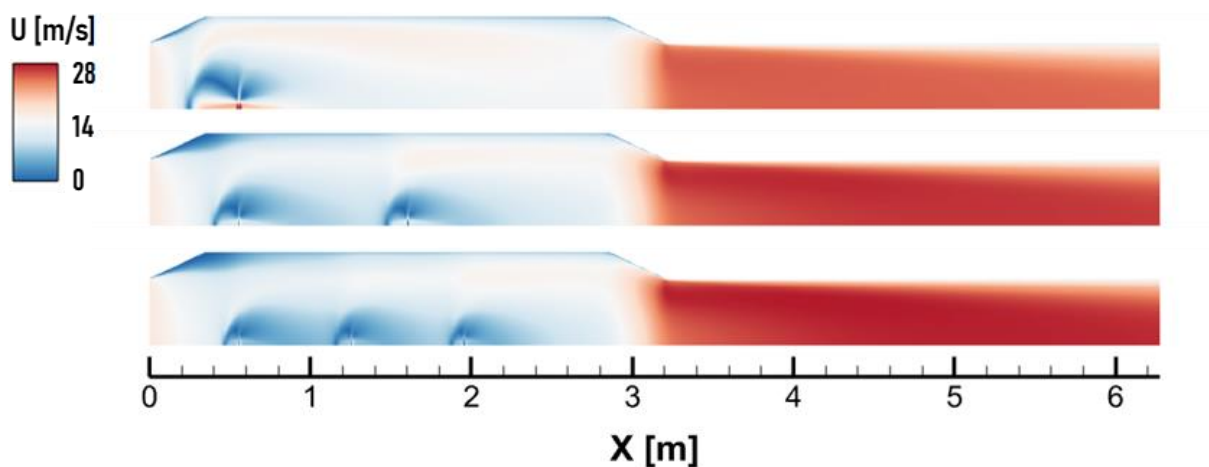


Figure 22. Contour plots of velocity magnitude in the cooled POC domain for 1, 2, or 3 oxygen injection stages.

The temperature fields in the case of POC equipped with a cooling system, for 1, 2, and 3 stages of oxygen injection, are presented in **Figure 21**. The temperature levels for all staging options are comparable, however, the location and the extent of the high temperature areas in the domain are affected. More oxygen injection stages lead to a small decrease in the volume of high-temperature cells in the domain. **Figure 22** provides information regarding the developed velocities within the chamber that rise to 28 m/s near the outlet, while **Figure 23** presents plots of the POC wall temperature for three oxygen staging options, revealing that the maximum numerically calculated temperature is approximately 850 °C. The heat removed from the domain by the cooling system was calculated to be from 217 to 335 kW, depending on the number of oxygen injection stages.

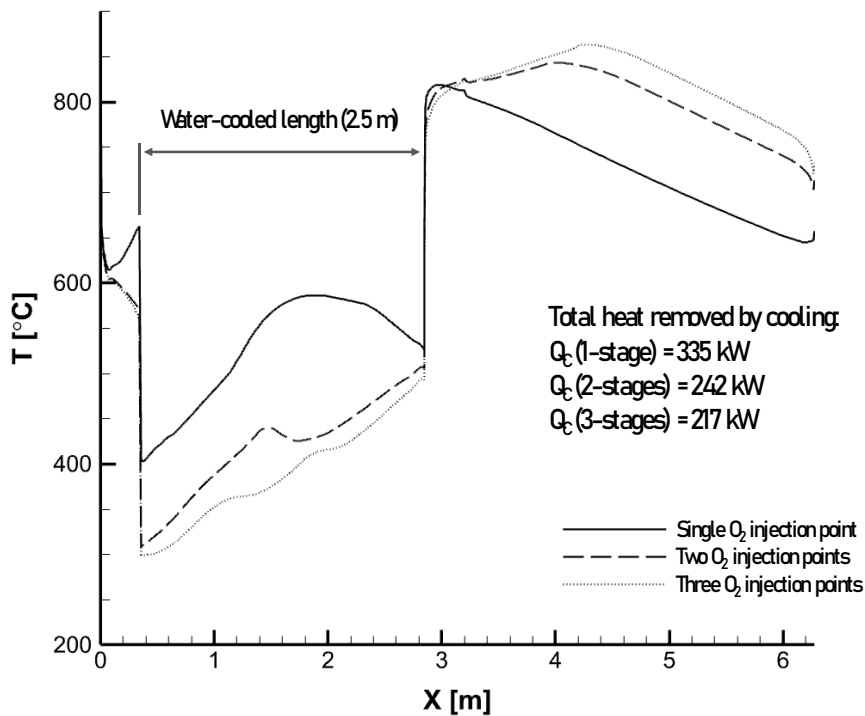


Figure 23. Line plots of cooled POC wall temperature along the length of the chamber for 1, 2, or 3 oxygen injection stages.

3.3.2. B – Refractory (adiabatic) wall

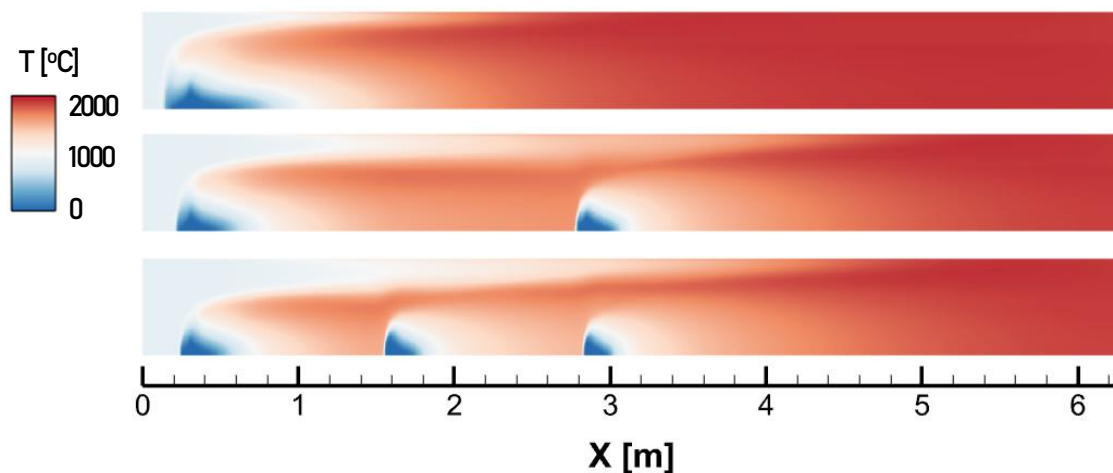


Figure 24. Contour plots of temperature in the adiabatic POC domain for 1, 2, or 3 oxygen injection stages.

The temperature fields for an adiabatic-wall POC, for 1, 2, and 3 stages of oxygen injection, are presented in **Figure 24**. It can be deduced that oxygen injection in stages leads to marginally lower temperature values in the domain. **Figure 25** provides information regarding the developed velocities within the chamber that rise to 44 m/s near the outlet, while **Figure 26** presents plots of the POC wall temperature for three oxygen staging options, revealing a maximum numerically calculated temperature of approximately 1900 °C.

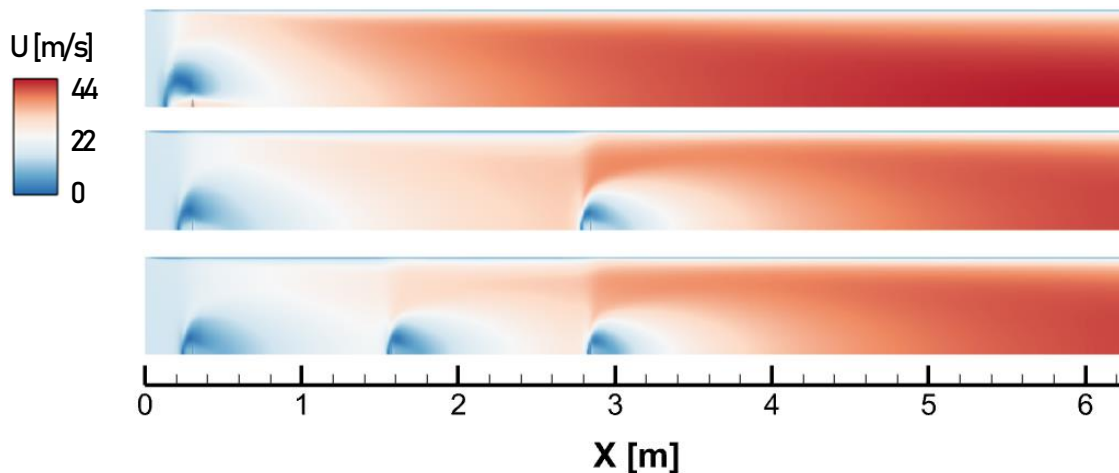


Figure 25. Contour plots of velocity magnitude in the adiabatic POC domain for 1, 2, or 3 oxygen injection stages.

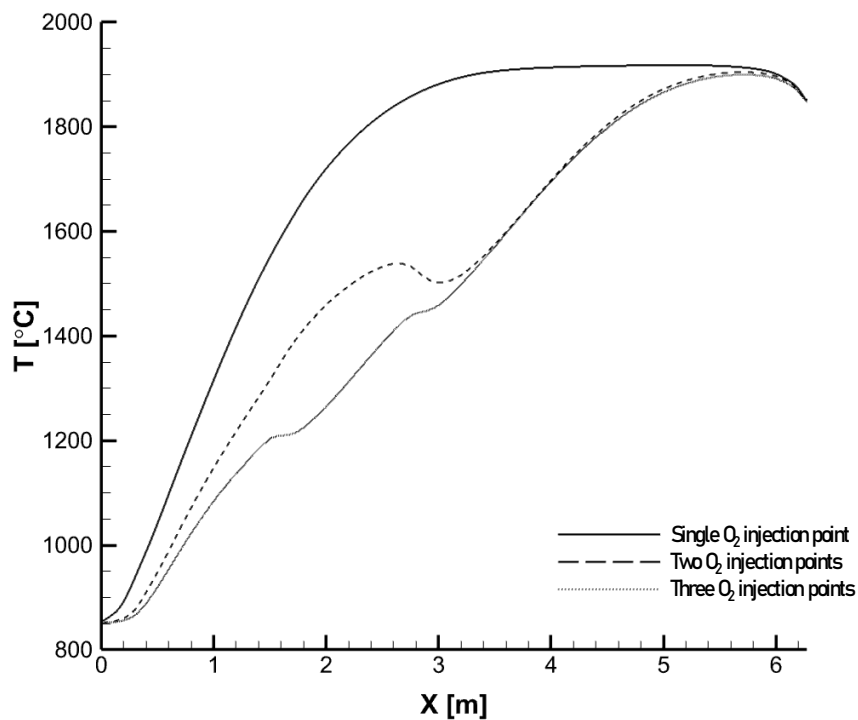


Figure 26. Line plots of adiabatic POC wall temperature along the length of the chamber for 1, 2, or 3 oxygen injection stages.

3.3.3. Comparative results

To evaluate the simulated cases and draw conclusions regarding the examined POC designs, the produced numerical results are presented in this section comparatively. More specifically, **Table 9** presents the total, numerically estimated heat produced by the oxidation for both proposed designs. The resulting values are in the range of 560 to 580 kW. Moreover, the heat that can be removed by the cooling system in the case of Design A, was calculated in the range of 220 to 340 kW. In the event of updated specifications regarding the cooling system, those calculations can be revisited and adjusted if necessary. Finally, **Table 10** contains the averaged values of temperature, velocity, and mole fractions at the outlet plane of each chamber. The introduction of a cooling system can maintain the outlet temperature lower than 1010 °C. On the contrary, outlet temperature from an adiabatic wall chamber is around 1900 °C.

Table 9. Total heat produced by the oxidation reactions inside the domain of the examined chambers and total heat removal by the cooling system of chamber design “A”.

Total domain value	Design A			Design B		
	Stages: 1	Stages: 2	Stages: 3	Stages: 1	Stages: 2	Stages: 3
Total heat of reaction [kW]	565	557	559	578	575	571
Heat removed by cooling [kW, (%)]	335 (59.3 %)	242 (43.4 %)	217 (38.8 %)	–	–	–

Table 10. Temperature, velocity and mole fraction averaged values at the outlet of the examined chambers.

Variable (value at the outlet)	Design A			Design B		
	Stages: 1	Stages: 2	Stages: 3	Stages: 1	Stages: 2	Stages: 3
$T [^{\circ}C]$	868	974	1009	1906	1900	1894
$U [m s^{-1}]$	18.7	20.5	21.1	36.7	35.6	34.8
$X_{C_2H_4} [-]$	0 %	0 %	0 %	0%	0%	0%
$X_{CH_4} [-]$	0.11%	0.12 %	0.09 %	0%	0%	0%
$X_{H_2} [-]$	0 %	0 %	0 %	0.11%	0.14%	0.18%
$X_{CO} [-]$	0.58 %	0.83 %	0.83 %	0.27%	0.38%	0.48%
$X_{CO_2} [-]$	27.61 %	27.35 %	27.37 %	27.97%	27.86%	27.75%
$X_{O_2} [-]$	6.30 %	6.36 %	6.31 %	6.20%	6.27%	6.33%
$X_{H_2O} [-]$	65.40 %	65.34 %	65.4 %	65.45%	65.35%	65.26%

4. CONCLUSIONS

This report summarized the work that was carried out by CERTH in cooperation with CSIC, CTH, and TUDA, in response to Task 2.2, titled “*CFD modelling of various designs for post-oxidation chamber*”. The goal of said Task, was the optimization of the post-oxidation chamber design by CFD modelling. To achieve this goal, CERTH developed a 2D-3D CFD model, employing both steady-state and transient RANS formulations, for the simulation of methane and ethylene oxidation inside an appropriate chamber. The geometries of the examined POC configurations were selected based on the needs and limitations that are present in the facilities of project partners CTH, CSIC, and TUDA. To model the methane oxidation process, a modified version of the Jones and Lindstedt [2] model was used. The model was modified for oxy-fuel combustion by Andersen et al. [4] In total, during the progress of improving the developed CFD model presented in this report, more than 10 different geometries and 50 sets of boundary and operating conditions were examined and analysed. The final numerical campaign contains data corresponding to 5 different geometries and more than 24 sets of operating conditions. The main findings that emerge from the CFD modelling vary depending on the case and operating conditions. Regarding the POC intended for the CHT facility, the numerical investigation concluded that injection of fuel and oxygen from the same side of the chamber leads to a more efficient chamber volume utilization. The CHT operating conditions result in low fuel supply in the chamber, and the oxidation process may not be self-sustained. In such low fuel supply conditions, chamber heat losses play an important role, and chamber insulation or introduction of a heating system may be necessary. The introduction of a heating system was examined in the case of the CSIC POC. Similarly, to CTH, the operating conditions of the CSIC facility led to a gas mixture containing a low concentration of combustible species. The numerically investigated heated POC design verified that the provided heat facilitated a faster and more efficient oxidation. However, in the case of a heated POC, oxygen staging was found not to play an important role in keeping the domain temperature low. Finally, in the case of the TUDA facility, where the gas mixture that will enter the POC is expected to have a higher content of combustible gases, the oxidation process was numerically found to be self-sustained. The produced heat was found adequate to raise the temperature higher than the desired threshold. In such high fuel supply cases, a cooling system is needed to keep the system temperature in control.

5. ABBREVIATIONS

CERTH	Centre for Research and Technology, Hellas
CFD	Computational Fluid Dynamics
CLC	Chemical looping combustion
CSIC	Spanish National Research Council
CTH	Chalmers University of Technology
DCKM	Detailed Chemical Kinetic Model
DO	Discrete ordinates
FR	Fuel reactor
POC	Post-oxidation chamber
RANS	Reynolds-averaged Navier-Stokes
SST	Shear stress transport
TUDA	Technical University of Darmstadt
WSGGM	Weighted-sum-of-gray-gases model



D2.3 - Optimization of the post-oxidation chamber design by CFD modelling

Proj. Ref.: Bio-FlexCLC-101147904
Doc. Ref.: Bio-FlexCLC-WP02-D2.3-DLR-CERTH-280525-V04
Date: 28/05/2025
Page N°: 26 of 26

6. REFERENCES

- [1] J. W. Gaertner, A. Kronenburg, A. Rees, J. Sender, M. Oschwald and G. Lamanna, "Numerical and experimental analysis of flashing cryogenic nitrogen," *International Journal of Multiphase Flow*, vol. 130, p. 103360, 2020.
 - [2] W. P. Jones and R. P. Lindstedt, "Global reaction schemes for hydrocarbon combustion," *Combustion and flame*, pp. 73(3), 233-249, 1988.
 - [3] C. K. Westbrook and F. L. Dryer, "Chemical kinetics and modeling of combustion processes," *In Symposium (International) on Combustion*, vol. 18, no. 1, pp. 749-767, 1981.
 - [4] J. Andersen, C. L. Rasmussen, T. Giselsson and P. Glarborg, "Global combustion mechanisms for use in CFD modeling under oxy-fuel conditions," *Energy & Fuels*, pp. 23(3), 1379-1389, 2009.
 - [5] N. Peters and B. Rogg, *Reduced kinetic mechanisms for applications in combustion systems (Vol. 15)*, Springer Science & Business Media, 2008.
-